High Precision Calibration Method for Binocular Visual System

Yuxin Du[1*], Minming Tong[2], He Zhang[3]

[1] School of Mechanical and Electrical Engineering, Xuzhou University of Technology, Xuzhou 221018, China
   duyuxinfish@outlook.com

[2] School of Information and Control Engineering, China University of Mining and Technology, Xuzhou 221008, China
   jctmm@163.com

[3] Architectural Design Institute China Jiangsu International Economic-Technical Cooperation Corporation, Xuzhou 221008, China
   499453547@qq.com

Abstract. For stereo vision systems, the accuracy of parameters calibration has a great influence on measurement and positioning precision in the later process. However, most existing calibration methods own shortcomings of low precision and high computation complexity, which can hardly be applied to occasions with strict measurement requirements. In this paper, we present an accurate camera calibration method for binocular systems based on geometric features of vanishing points formed by two sets of parallel lines. Based on the central symmetry, the position of distortion center is firstly calculated out. Then we treat it as the initial value and utilize genetic algorithm to optimize distortion parameters by minimizing straight degrees of corrected lines, which greatly reduces the algorithm computational complexity. After calibrating internal parameters with the proposed method, external parameters are figured out on the basis of geometric properties of orthogonal vanishing points. Finally, geometry constraint between epipolar lines is adopted for optimizing structure parameters of the binocular system by minimizing matching errors under different views. It significantly improves the algorithm robustness and re-duces noise interference. Experimental results show that the proposed method with impressive precision and stability can exactly finish the parameters calibration for stereo systems.

Keywords: binocular visual system, camera calibration, camera modelling, parameters optimization

1   Introduction

With the rapid development of computer technique, stereo vision technology has been gradually applied in many industry fields for improving production efficiency and automatic degrees. The calibration of camera parameters is the most basic and important part, whose reliability and accuracy will directly affect the stability and precision of the whole system. Although many scholars had proposed a series of classical calibration methods and tools, traditional methods still need to be modified for practical measurement applications in order to improve the calibration accuracy and realize the accurate 3D space reconstruction. The calibration of a binocular system includes two steps, internal and external parameters calibration of monocular cameras and the structural parameters calibration between them.

According to different camera models, existing monocular calibration can be classified into linear and nonlinear methods. Without consideration of lens distortion, results of linear methods [1] generally can hardly meet the requirement of high calibration precision. At present, most nonlinear methods [2-3]

---

* Corresponding Author

choose feature points around the image center to complete the camera's linear calibration in the first place, and then optimize them with iterative algorithms, which is complex, time-consuming and can hardly avoid local optimization. Somewhat differently, our method firstly gets the exact location of the camera distortion center and then uses it to optimize other distortion parameters. In this way, it successfully avoids the appearance of local optimum and improves the calibration efficiency.

After obtaining lens distortion parameters, the calibration of internal and external parameters is needed in the next step. Traditional methods [4-5] calculate various parameters for a camera by using high precision 3D templates with expensive cost and complex manufacture. In contrast, self-calibration techniques [6-7] exploit motions of camera and surrounding environments for calibration. Since the poor robustness and complicated operation, they are mainly used in those fields with no requirements for high accuracy. By combining advantages of traditional and self-calibration methods, Zhang [8] proposed a calibration chessboard in 2000 with simple operation and wide applying foregrounds. It had become one of the most commonly used calibration templates in the field of machine vision [9]. However, these methods usually require multiple images since they have to sample a planar pattern from different views, which increases the computation complexity. With affluent mathematical and geometric properties, the calibration technique based on vanishing points [10] has been widely used since being put forward in 1990 [11]. At present, most of these methods take coordinates of circular points [12] or position relation between vanishing points and the image of the absolute conic (IAC) [13] as the transition value to estimate the fundamental matrix indirectly. For reducing algorithm complexity, our method calibrates internal and external parameters separately. All of the internal parameters can be linearly figured out by using lines on the template with known dimensions. Afterwards, it directly figures out external parameters according to geometrical relationship between the image of parallel lines and camera center.

After monocular camera calibration, parameters of binocular system need to be optimized for improving the measurement accuracy. With images of a coded template under different views, Li et al. [14] employed the alternative bundle adjustment between stereo images to optimize structure parameters. It is obvious that existing methods always report on parameters optimization based on 2D image plane by minimizing errors between re-projected points and the real ones. However, different optimization and measurement coordinate systems may cause precision reduction. To solve this problem, with the appearance of epipolar geometry constraint theory, some researches have been developed based on spatial constraints between stereo images. For example, Kumar [15] utilized constraint errors to eliminate redundant nodes, which decreases calibration time and simultaneously reduces reconstruction errors. Zhang et al. [16] calibrated a vision system consisting of four fish eye lenses and used the epipolar correction method for parameters optimization. Due to the existence of two images of the same objects at different views, we could find that the imaging point of a spatial point in the left picture is exactly on the epipolar line in the right. Hence, in this paper, we propose an optimization method to binocular system to improve the measurement accuracy by considering the epipolar constraint that represents the position of one point referred to its corresponding point in the other image.

Table 1. Comparison table of related works in recent years and the proposed method

Study	Reference objects	Camera model	Calibration principle	Optimization procedure
Boudine et al. (2016)	Self-calibration	Linear	IAC	Epipolar geometry
Yang et al. (2016)	Collinear points	Nonlinear	Spatial point constraints	Reprojection errors
Semeniuta (2016)	Chessboard	Nonlinear	Zhang's method	Reprojection errors
Sun et al. (2012)	Calibration cross	Nonlinear	3D points set	None
Xu et al. (2014)	Self-calibration	Nonlinear	Vanishing points	None
Zhang et al. (2000)	Chessboard	Nonlinear	IAC	Reprojection errors
Lu et al. (2014)	Chessboard	Linear	Vanishing points	Tsai's two steps
Zhao et al. (2016)	Self-calibration	Linear	Circular points	None
Liu et al. (2014)	Chessboard	Nonlinear	IAC	Reprojection errors
Li et al. (2017)	Special encoded template	Nonlinear	Epipolar geometry	Alternative bundle adjustment
Kumar et al. (2016)	Chessboard	Linear	Epipolar geometry	None
Zhang et al. (2015)	Dot lattice	Nonlinear	Epipolar geometry	None
Proposed	Parallel lines	Nonlinear	Vanishing points	Epipolar constraint

In view of above shortcomings of existing methods, as shown in Table 1, an effective calibration method with high accuracy and low complexity is needed for binocular system. In this paper, we finish

the stereo calibration based on characteristics of distorted lines and geometric properties of vanishing points of lines on the two-dimensional (2D) template, which owns advantages of easy realization, high precision and outstanding robustness.

The remainder of this paper is structured as follows. In Section 2, after camera modeling, the distortion center of a camera is achieved through curves fitting according to the central symmetry feature of distorted images. In Section 3, for reducing iterations, straight degrees of curves are viewed as the nonlinear objective function to optimize distortion parameters with the earned distortion center as the initial value. Afterwards, a linear calibration method is put forward to get intrinsic parameters of binocular cameras. In Section 4, a novel method is proposed to work out and optimize extrinsic parameters on the basis of geometric properties of two orthogonal vanishing points in space. On account of simple principle, there is no need of Cholesky decomposition, which greatly reduces the computational complexity of our algorithm. In Sections 5 and 6, we take monocular and binocular calibration experiments to verify the calibration effects and precision of our method by comparing it with others. Finally, we conclude this paper and point out possible future works in Section 7.

2 Monocular Model

2.1 Camera Model

Camera models describe mapping relations between spatial points and points on the image, which can be a pinhole model without consideration of lens distortions. The projection from a spatial point $P_w = (X_w, Y_w, Z_w, 1)^T$ in the world coordinate system $(O_w\text{-}X_wY_wZ_w)$ to the image point $p = (u, v, 1)^T$ in the image coordinate system $(O_p\text{-}uv)$ is

$$s\begin{bmatrix} u \\ v \\ 1 \end{bmatrix} = K\begin{bmatrix} R & T \end{bmatrix}\begin{bmatrix} X_w \\ Y_w \\ Z_w \\ 1 \end{bmatrix},\tag{1}$$

where s is the proportionality coefficient, K is the internal parameters matrix of the camera, $[R\ T]$ is the external parameters matrix. Furthermore, R and T are the rotation matrix and translation vector of the camera relative to the world coordinate system, respectively. The expression of K is as follows

$$K = \begin{bmatrix} f_x & \alpha & u_0 \\ 0 & f_y & v_0 \\ 0 & 0 & 1 \end{bmatrix}, \begin{cases} f_x = f/d_x \\ f_y = f/d_y \end{cases},\tag{2}$$

where (u_0, v_0) are coordinate values of the image central point in the image coordinate system, f is the focal distance of the camera, d_x and d_y are actual dimensions of each pixel in x and y axes, f_x and f_y are scale factors of the image, α is the inclination factor which is zero in general.

2.2 Distortion Model

Owing to imperfect production, optical sampling of lens is difficult to be idealized, which would cause the image distortion, such as radial, tangential and thin lens distortions. Hence, distortion models are introduced into the camera imaging model, since the inaccurate description of the pinhole model.

Definitions of the image central point are not the same in different camera models. In the perspective projection model, the center is defined as the intersection of the optical axis and the imaging plane. However, in camera distortion model, it is deemed to be the distortion center of the image. Fortunately, these two positions keep consistent when radial distortion is considered only. Tsai and Lenz [4] pointed out that the introduction of a nonlinear model can improve the accuracy of calibration. However, if the model contains too many nonlinear parameters, it would be extremely easy to destabilize the results and decrease calibration precision.

Therefore, in order to exhibit the actual lens distortion and improve accuracy, this paper only considers impacts of radial and tangential distortions on images. The distortion of a camera is applied based on two

and four powers of the viewing field angle θ [17]. Expressions are shown as below,

$$\begin{cases} u = u_d + \Delta u(k_1\theta^2 + k_2\theta^4) + p_1(r^2 + 2\Delta u^2) + 2p_2\Delta u\Delta v \\ v = v_d + \Delta v(k_1\theta^2 + k_2\theta^4) + p_2(r^2 + 2\Delta v^2) + 2p_1\Delta u\Delta v \end{cases}, \tag{3}$$

$$\Delta u = u_d - u_0, \Delta v = v_d - v_0, r = \sqrt{\Delta u^2 + \Delta v^2}, \theta = \arctan(r/f), \tag{4}$$

where (u_d, v_d) are coordinates of a point on distorted image, (u, v) are its values without distortion, (u_0, v_0) are coordinates of the distortion central point, k_1 and k_2 are radial distortion coefficients, p_1 and p_2 are tangential distortion parameters, Δu, Δv and r are horizontal, vertical and straight-line distances between a point on the image and the distortion center, respectively, and f is the focal distance which is 6mm in this system.

3 Non-metric Internal Parameters Calibration for Monocular Camera

3.1 Distortion Center Point Calibration

For increasing accuracy, image geometric center cannot be roughly regarded as the distortion center. Therefore, complex nonlinear methods are usually employed, which greatly increase the computation complexity. In this paper, before calibrating other parameters, location of the distortion center (u_0, v_0) is firstly figured out based on the centrosymmetry of image distortion by using the method of deformed curves fitting. Then, variables in the nonlinear objective function are optimized by taking achieved distortion center (u_0, v_0) as initial values. It can effectively improve the calibration efficiency and reduce iterations of the optimization algorithm. In general, Zhang [8] chessboard is utilized as the calibration template [18]. Similarly, a plane template shown in Fig. 1 is adopted in this paper, which can be easily obtained by normal printing.
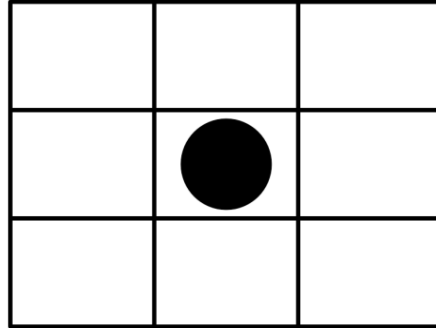

Fig. 1. Calibration template

In Fig. 2, L_1 and L_2 are undistorted straight lines which intersect each other. Curves C_1 and C_2 are images of L_1 and L_2 in the deformed picture. According to the property that the distortion satisfies central symmetry, all straight lines will be distorted into curves with their symmetric lines passing through the camera central point. Hence, in this paper, misshapen lines at different positions are fitted by Gaussian curves with the expression of $y = y_0 + A/\sqrt{2\pi}\sigma \exp[-(x - x_r)^2/(2\sigma^2)]$. The centrosymmetric point B_1 (B_2) $(x_r, y_0 + 2\sqrt{\pi}\sigma)$ of the Gaussian curve is just the symmetric center point of C_1 (C_2). After these, symmetrical central lines B_1O and B_2O can be calculated out. Their intersection is the distortion center point O (u_0, v_0). In this paper, in order to reduce fitting errors, all eight distortion curves are considered, and the mean value is seen as the final distortion center.
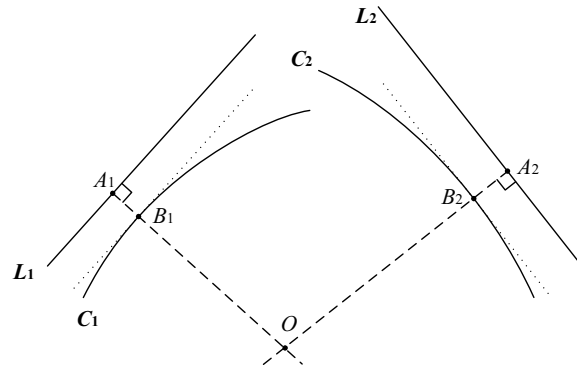
Fig. 2. Calibration of distortion center point

3.2 Distortion Parameters Optimization

In this paper, we assume that initial values of k_1, k_2, p_1, p_2 in Eq. (3) are both zero. After being corrected, a point (u_d, v_d) in the distorted image turns into the point (u'_d, v'_d). A curve C_d becomes the curve C'_d. The closer to real values distortion parameters are, the straighter curve C'_d is. For this reason, the straight degree of C'_d reflects the extent of distortion parameters approaching true values.

Using a line L to connect start and end points of a curve, the sum of areas enclosed by L and the curve can be expressed as a distortion level to judge the correction result. After rectification, shapes of curves may be convex, concave or even sigmoid. When it is sigmoid, the original curve would be divided into parts by the line L, which easily makes separated areas offset with each other during calculation. Then the final result will be smaller than actual value. Consequently, summation of small trapezoid areas is exploited to achieve the total area with the representation of

$$\xi(k_1, k_2) = \sum_{i=1}^{M} A_i^2 = \sum_{i=1}^{M} [\sum_{j=2}^{N_j} (\frac{d_i^{j-1} + d_i^j}{2}) d_i^{j-1,j}]^2 , \qquad (5)$$

where d_i^j is the vertical distance from point j on curve i to line L, $d_i^{j-1,j}$ is the distance of the connected line between points j-1 and j on curve i projected onto L.

The shape of a curve after correction is unknown, which is completely related to values of distortion parameters. Therefore, Eq. (5) is chosen as the object function in parameters optimization to gain global optimum solutions of distortion parameters k_1, k_2, p_1, p_2, u_0 and v_0. Genetic algorithm owns advantages of global optimization, high precision and strong robustness. Hence, this paper takes use of the genetic algorithm in MATLAB Optimization Toolbox to search global optimization values of distortion parameters. Since the uncomplicated operation, depictions of this toolbox are omitted here. After that, accurate correction can be done only with easily obtained straight lines.

3.3 Internal Parameters Calibration

The image after distortion correction can be considered as an ideal undistorted image, which accords with the pinhole model [18]. Based on this, exterior and interior parameters of a camera can be linearly calibrated. It gets parameters on a calibration table, which avoids shortcomings of traditional methods, such as tedious operation, complex algorithm and so on. As shown in Fig. 3, the target keeps perpendicular to the orbit on the platform and can move along it. Binocular system is also adjusted, in which two optical axes keep parallel to the rail.
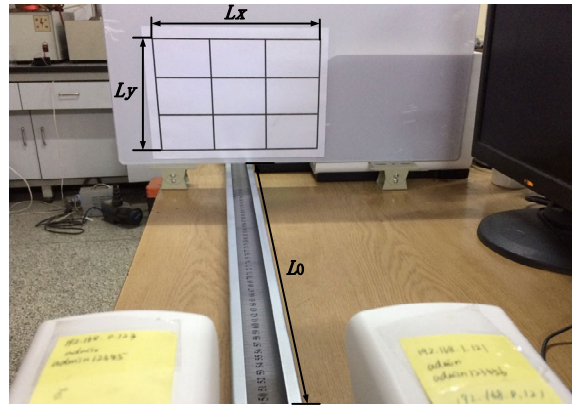
Fig. 3. Internal parameters calibration table

Before calibration, sizes of the target are known. Horizontal and vertical sides of the template are named as L_x and L_y. Pixels of it on the image are N_x and N_y. The distance between the target and the camera is L_0. f is the camera focal distance. According to Eq. (2) and the geometric relationship in Fig. 4, there is

$$\begin{cases} f_x = f / dx = L_0 \times N_x / L_x \\ f_y = f / dy = L_0 \times N_y / L_y \end{cases}. \tag{6}$$
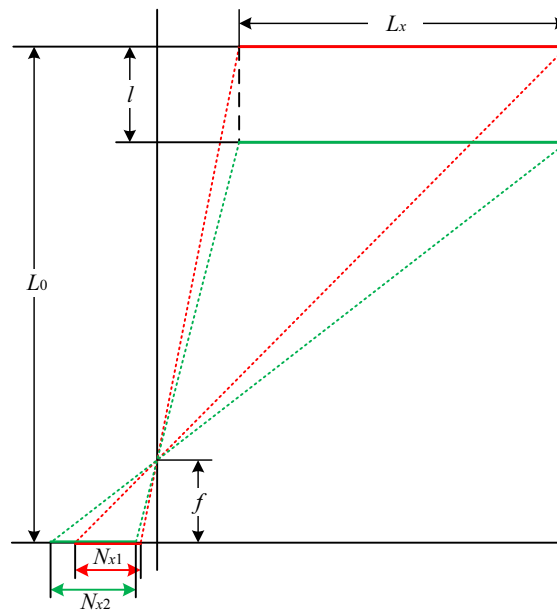

Fig. 4. Diagram of image formation

By solving simultaneous equations of the target at two different positions, we can get

$$\begin{cases} N_{x_1} dx / Lx = f / L_0 \\ N_{x_2} dx / Lx = f /(L_0 - l) \end{cases}, \tag{7}$$

where N_{x1} and N_{x2} are image pixels of L_x at different distance. Then, L_0 can be figured out

$$L_0 = l N_{x_2} /(N_{x_2} - N_{x_1}). \tag{8}$$

By substituting Eq. (8) into Eq. (6), internal parameters f_x and f_y can be gained. So far, using above method, left and right cameras can be exactly calibrated, inner matrixes K_l and K_r can also be obtained.

4 Structural Parameters Calibration for Binocular System

4.1 External Parameters Calibration

External parameters include rotation $\boldsymbol{R}$ and translation matrices $\boldsymbol{T}$ between the world and camera coordinate systems. In this paper, $\boldsymbol{R}$ is firstly solved base on vanishing points geometric properties of two sets parallel lines which are orthogonal with each other in space. The optical center of camera is just located on the surface of a sphere with the connecting line between two vanishing points as its diameter.

As shown in Fig. 5, lines $L_1//L_2$, $L_3//L_4$, $L_1 \perp L_4$, imaging lines l_1 and l_2 of L_1 and L_2 on the picture intersect at the vanishing point A, l_3 and l_4 intersect at point B. Thereby, lines O_cA and O_cB parallel to L_1, L_4, respectively. Then, there is $O_cA \perp O_cB$. The optical center O_c is located on a spherical surface with AB as its diameter.
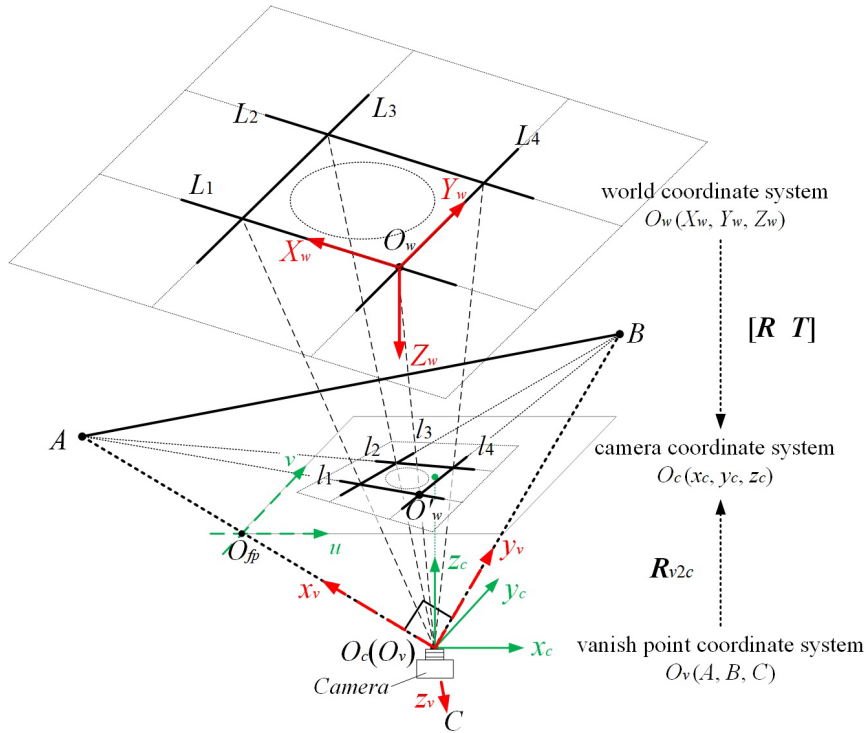

Fig. 5. Geometric projection model of two orthogonal sets of parallel lines

The world coordinate system O_w (X_w, Y_w, Z_w) is set up with intersection O_w of orthogonal lines L_1 and L_4 as the original point, vectors O_wL_1 and O_wL_4 as x and y axes. Similarly, the camera coordinate system O_c (x_c, y_c, z_c) can also be established with the optical center O_c of the camera as its original point, camera optical axis as its z_c axis, in which x_c and y_c axes are both parallel to the image plane. $\boldsymbol{R}$ is the rotation matrix between systems O_w (X_w, Y_w, Z_w) and O_c (x_c, y_c, z_c). According to geometric properties of orthogonal vanishing points, there are $O_cA//L_1$ and $O_cB//L_4$. For the sake of calculating out $\boldsymbol{R}$, the origin O_c of the world coordinate system is moved to O_v. The vanishing points coordinate system O_v (A, B, C) is set up with O_vC (z_v axis) keeping parallel to the Z_w axis. Thereafter, regarding O_v (A, B, C) as the transition coordinate system, the rotation information between O_c (x_c, y_c, z_c) and O_v (A, B, C) can be calculated out.

In the image coordinate system (O_p-uv), coordinates of vanishing points A, B are (u_A, v_A), (u_B, v_B). (u_0, v_0), fx and fy have already been obtained in Sec. 3. Then, there are $\boldsymbol{O_vA} = [(u_A - u_0) f /f_x, (v_A - v_0) f /f_y, f]^T$, $\boldsymbol{O_vB} = [(u_B - u_0) f /f_x, (v_B - v_0) f /f_y, f]^T$, $\boldsymbol{O_vC} = \boldsymbol{O_vA} \times \boldsymbol{O_vB}$. For the reason that O_v (A, B, C) is translated from the position of O_w (X_w, Y_w, Z_w), normalized vectors [a, b, c] of $\boldsymbol{O_vA}$, $\boldsymbol{O_vB}$, $\boldsymbol{O_vC}$ are parallel to X_w, Y_w, Z_w axes. In consequence, in O_v (A, B, C), the three-dimensional vector composed by axes X_w, Y_w and Z_w is a unit matrix $\boldsymbol{I}$. The rotation matrix $\boldsymbol{R}_{v2c}$ can be employed to transform these two systems, where [a, b, c] $= \boldsymbol{IR}_{v2c}$, namely $\boldsymbol{R}_{v2c} = [a, b, c]$. However, $\boldsymbol{R}_{v2c}$ is not necessarily equal to the rotation matrix $\boldsymbol{R}$. Direction

relations between O_w (X_w, Y_w, Z_w) and O_v (A, B, C) need to be judges owing to the fact that vectors on two parallel lines may be identical or contrary to each other. The projected point of O_w on the imaging plane is O_w' (u_w, v_w). R can be confirmed by determining direction relations between O_w'A, O_w'B and axes x_w, y_w.

Supposing there is a point P_w in the world coordinate system with coordinate values of (X_w, Y_w, Z_w), the translation matrix T between O_w (X_w, Y_w, Z_w) and O_c (x_c, y_c, z_c) can be solved according to Eq. (1).

4.2 External Parameters Optimization of Binocular Cameras Based on Epipolar Geometry Model

To a binocular stereo measuring system, it is important to calibrate not only monocular parameters, but also relative positions between two cameras. R_{l2r} and T_{l2r} are used to represent rotation and translation matrices of the movement from left to right camera systems, which are named collectively as external parameters. There is

$$X_r = R_{l2r}X_l + T_{l2r} , \tag{9}$$

where X_r and X_l are coordinate values of a same point in right and left coordinate systems, respectively. After calibration in Sec. 3, [R_l T_l], [R_r T_r] are known. There is

$$\begin{cases} R_{l2r} = R_r R_l^{-1} \\ T_{l2r} = T_r - R_r R_l^{-1} T_l \end{cases} . \tag{10}$$

Following formula is the epipolar equation of binocular images defined by the epipolar geometry

$$\begin{cases} l_r = F p_l \\ l_l = F^T p_r \end{cases} , \tag{11}$$

where p_l and p_r are projective points homogeneous coordinates of point P in 3D space on imaging planes of two cameras, respectively, F is the fundamental matrix which reflects projection of P in the camera coordinate system at different views with the expression of

$$F = K_r^{-T}[T_{l2r}]_\times R_{l2r} K_l^{-1} . \tag{12}$$

Structural parameters R_{l2r} and T_{l2r} remain unchanged at different views owing to the stable binocular structure. According to the epipolar geometry constraint, the imaging point of a spatial point in the left picture must be on an epipolar line in the right. There is $p_l^T F^T p_r = 0$ or $p_r^T F p_l = 0$. Therefore, R_{l2r}, T_{l2r} are optimized by using Levenberg-Marquardt optimization algorithm with Eq. (13) as the objective function.

$$er = \frac{1}{N}\sum_{i=1}^{N}(\frac{1}{M_i}\sum_{j=1}^{M_i}\left| p_{r_j}^T F p_{l_j} \right|) , \tag{13}$$

where N is the total number of camera views, M_i is number of matched characteristic points which are obtained by SURF algorithm at view i. Finally, we can obtain the structure parameters of the binocular visual system.

5 Monocular Calibration Experiments

5.1 Distortion Calibration of Synthetic Image

For the sake of verifying the accuracy of this distortion calibration algorithm, we firstly use the synthetic templet with 300×400 pixels as shown in Fig. 6(a). Assuming distortion parameters $k_1 = -0.3$, $k_2 = 0.2$, $p_1 = -0.001$, $p_2 = -0.002$, $u_0 = 150$, $v_0 = 200$, the distorted image without noise can be created through (3) for the next calibration, which is shown in Fig. 6(b). After that, in order to imitate actual situations, Fig. 6(b) is destroyed to be Fig. 6(c) by Gauss white noise with standard deviation of σ.
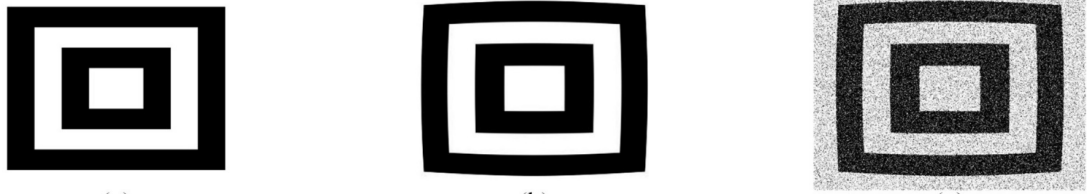
| (a) without noise and distortion | (b) with distortion | (c) with noise and distortion |

Fig. 6. Synthetic images

The proposed algorithm in Sec.3 is used to deal with distorted images under different Gauss white noises. Thereafter we can obtain percentage errors of four distortion parameters, as shown in Fig. 7. In view of the steadiness of p_1 and p_2, their values are not exhibited here. Percentage errors of (u_0, v_0) increase slower with the growth of noise than that of k_1 and k_2. This is because that the location of the distortion center point has already been estimated before the optimization of distortion parameters, which reduces the pixels error and iterations of this optimization algorithm. When the Gauss noise variance is 0.12, errors of four parameters are all smaller than 8%. The location error of the center point is less than 6 pixels. These show that the proposed method can well estimate values of image distortion parameters and meet requirements of accurate calibration.
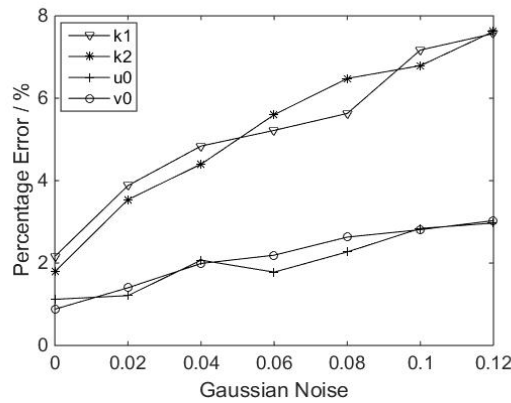

Fig. 7. Calibration results of synthetic distortion image

5.2 Distortion Calibration of Sampled Image

Cameras experimented here are mine-used explosion-proof ones with lens produced by the *HIK Vision Company*. Their focal lengths are both 6mm. By taking the left camera for example, we correct distorted images of the template (shown in Fig. 1) under 16 different views. Fig. 8 exhibits the calibration results.

Data in Fig. 8 are values of (a) u_0 and v_0, (b) k_1 and k_2, (c) p_1 and p_2, (d) iterations, (e) object function after distortion correction of 16 different images. As can be seen from these curves, the difference of each parameter obtained from different images is not large, which illustrates that the proposed algorithm is reliable and robust.

In order to further certify the correction effect of this algorithm, it is necessary to acquire the distance between the corrected position and the real position of each characteristic point. However, real values of camera intrinsic parameters cannot be earned ideally. Neither can real positions of characteristic points. Therefore, average values are taken as joint correction values here to make them closer to real ones. And the corrected image is used as the reference. After this, a pixel point (i, j) in the original image can be corrected with the joint correction values to be (x''_{ij}, y''_{ij}). (x'_{ij}, y'_{ij}) is the location of (i, j) after the proposed method. Eq. (14) describes root-mean-square (RMS) of the distance between (x''_{ij}, y''_{ij}) and (x'_{ij}, y'_{ij}),

$$Dis = \sqrt{\sum_{j=1}^{N} \sum_{i=1}^{M} [(x''_{ij} - x'_{ij})^2 + (y''_{ij} - y'_{ij})^2]/(M \times N)} \, , \tag{14}$$
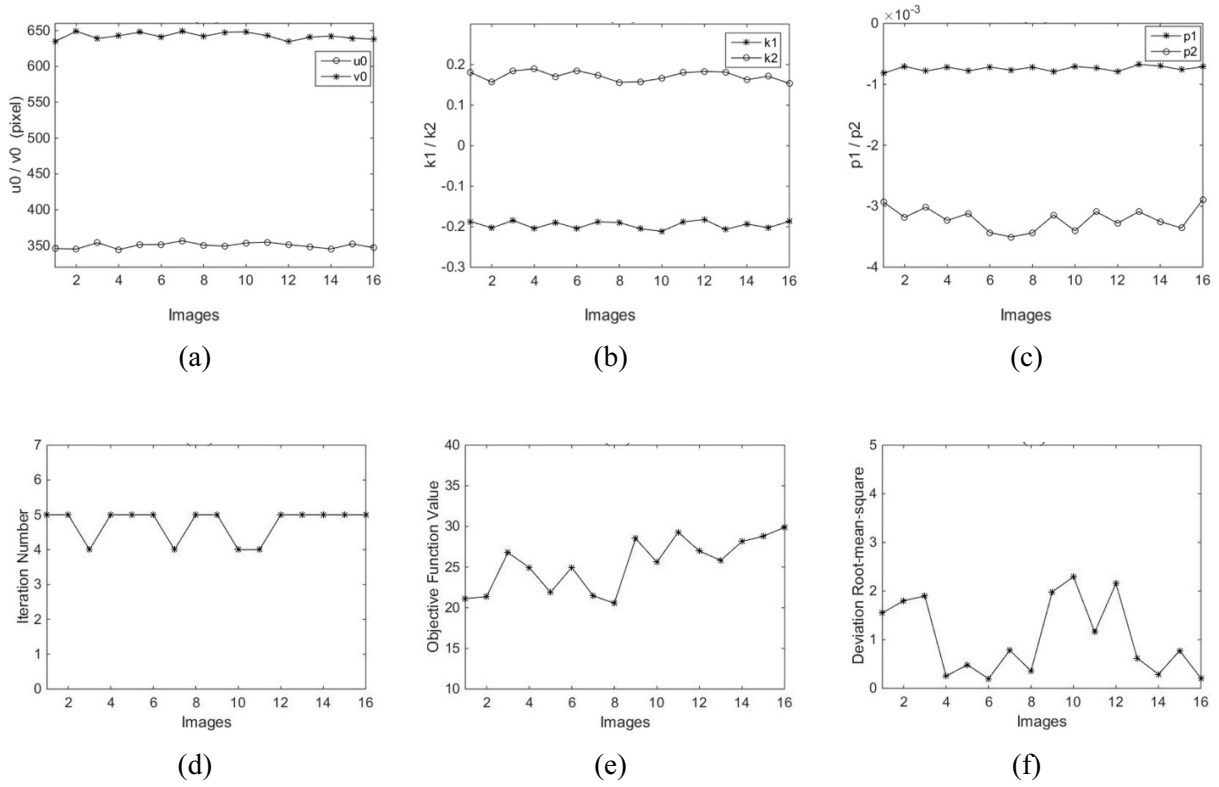
(a)   (b)   (c)

(d)   (e)   (f)

Fig. 8. Calibration results of sampling distorted image.

where N is the number of acquired images, M is the number of characteristic points in each image. Fig. 8(f) shows the RMS between experiment values and real ones, which are all within 3 pixels. This illustrates that correction results of different images are essentially similar to each other and the algorithm in this paper is extremely robust. Finally, we can get distortion parameters of the left camera, $k_1 = -0.19597$, $k_2 = 0.03283$, $p_1 = -0.00075$, $p_2 = -0.0032$, $u_0 = 388.21278$, $v_0 = 611.3357$. Similarly, those of the right can be obtained as $k_1 = -0.18193$, $k_2 = -0.04945$, $p_1 = -0.00069$, $p_2 = -0.0038$, $u_0 = 385.35727$, $v_0 = 609.03653$.

Afterwards, multiple groups of images are sampled in different positions. In accordance with the method in Sec. 3, other two internal parameters fx and fy are figured out after the distorted images correction. In this way, we can acquire internal parameter matrices of left and right cameras, $\boldsymbol{K_l} =$

$$\begin{bmatrix} 1566.11165 & 0 & 388.21278 \\ 0 & 1568.72528 & 611.3357 \\ 0 & 0 & 1 \end{bmatrix}, \boldsymbol{K_r} = \begin{bmatrix} 1569.92003 & 0 & 385.35727 \\ 0 & 1574.50549 & 609.03653 \\ 0 & 0 & 1 \end{bmatrix}$$

6   Binocular Calibration Experiments

6.1   External Parameters Calibration and Re-projection Errors Analysis

The binocular vision system used in this test is composed of two cameras of the same type with the horizontal distance of around 145.5mm. 24 groups of images are collected by this system. Adopting the method in Section 4, external parameters of left and right cameras are calculated out by treating the top left corner point on the calibration template as the origin of the reference coordinate system. So are locations of 16 marked points after distortion correction. These 16 spatial points are then re-projected onto 24 groups of images with above obtained camera parameters to get errors between projected points and actual ones, which are shown in Fig. 9. As can be seen, the re-projection errors of two cameras are all in the range of [-0.2, 0.2] pixels and mostly concentrate in [-0.05, 0.05] pixels.

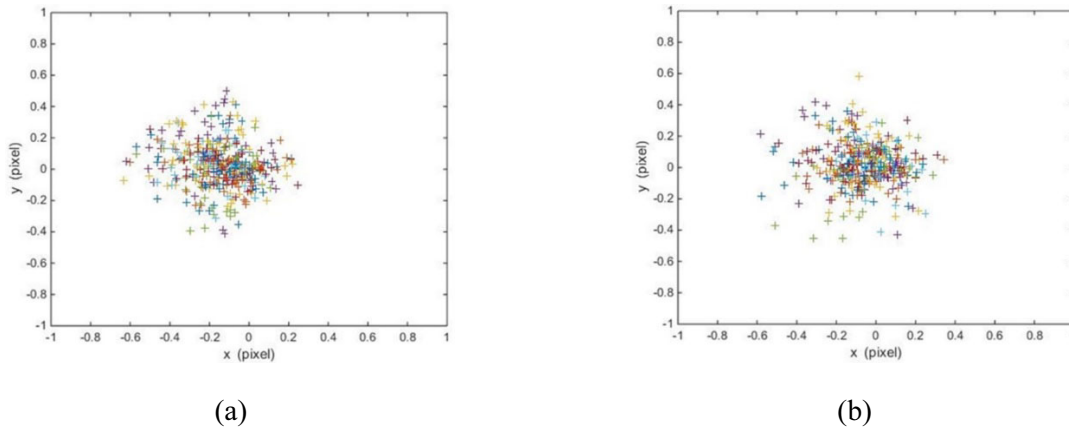(a)   (b)

Fig. 9. Re-projection errors of (a) right, (b) left cameras

For the purpose of quantifying the accuracy of the proposed algorithm, the performance of this re-projecting operation is demonstrated by values of mean, standard deviation (STD), RMSE and maximal values on x and y axes respectively, which are listed in Table 2. The average re-projection errors of two cameras are both within 0.06 pixels, values of STD and RMSE also meet requirements of precise measurement, which states that our method with high accuracy is practical.

Table 2. Re-projected errors of characteristic points (in pixels)

		Mean	STD	RMSE	Max
Right camera	x axis	0.0559	0.0106	0.0705	0.2109
	y axis	0.0371	0.0090	0.0497	0.1673
Left camera	x axis	0.0418	0.0113	0.0541	0.1936
	y axis	0.0357	0.0075	0.0486	0.1933

6.2   Binocular Calibration and 3D Reconstruction Errors Analysis

After gaining the rotation matrix R_{l2r} and translation matrix T_{l2r} between two cameras, Eq. (14) is taken as the objection function to optimize them. Results are $R_{l2r} = \begin{bmatrix} 0.9999 & -0.0053 & -0.0153 \\ 0.0048 & 0.9993 & -0.0370 \\ 0.0155 & 0.0370 & 0.9992 \end{bmatrix}$, T_{l2r} = [-0.14558, 0.00044, -0.00039] m.

Effectively, the relative pose between two cameras is almost translation only. Therefore, the obtained rotation matrix is close to an identity matrix. The first value in T_{l2r} represents the distance between optical centers of two cameras, which is 145.58mm. And the actual measurement value is around 145.5 mm. This calibrated external parameter is very close to the fixed physical parameter of the binocular system.

From images collected by this binocular system, it is easy to get measured 3D coordinate values of spatial points that can be compared with actual ones. In Fig. 10, there are only comparison results on x and y axes as a result of the fact that reconstructed coordinate values of signalized points are almost zero on the z axis. In above figure, "○" expresses physical locations of 16 target points on the temple and "+" indicates measured values of them in 24 groups of images, which are almost completely coincident.

For analyzing three-dimensional reconstruction errors of spatial points, distances between points ① and ⑯ after reconstruction are measured and compared with the actual range 236.56mm. Measurement errors of these stereo images are all within 0.3mm, the average error is 0.0913mm, the maximum error is 0.1621mm and the standard deviation is 0.0536mm. After this, an accuracy comparison of the proposed method with others, Cui [19], Sun [20] and calibration toolboxes in Matlab and OpenCV, is done as Table 3 shows. Actual measure distances of Cui method, Matlab and OpenCV are all 243.02mm. The result of Sun is directly obtained from the reference. After obtaining absolute errors, relative ones are figured out afterwards. We can find that calibration toolboxes in Matlab and OpenCV hold similar results

above 0.5%. Cui is better than them. Sun and the proposed one own ideal error which is less than 0.1%. Compared with other methods, the proposed method shows accurate results with higher efficiency, which satisfies needs of precious measuring and can complete the accurate reconstruction of 3D space.
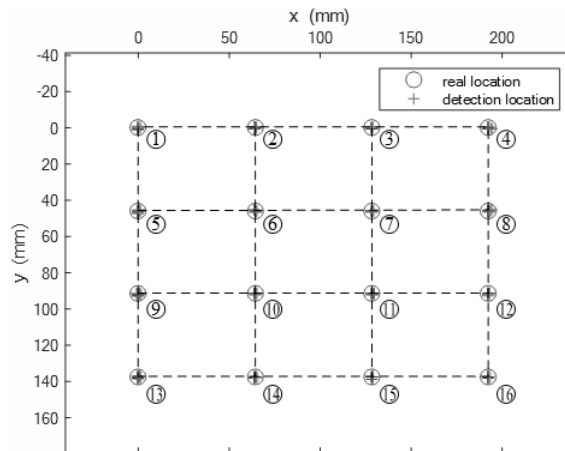

Fig. 10. Actual coordinate values and 3D reconstruction ones of 16 spatial points
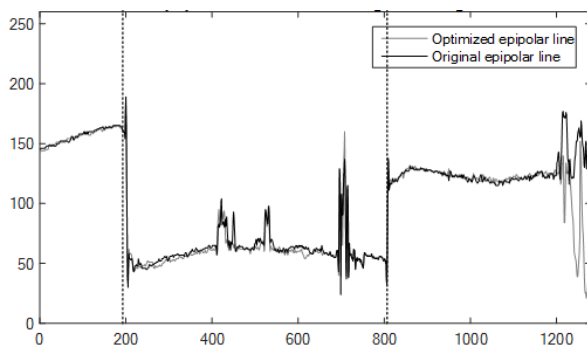
Table 3. Measurement errors of standard length

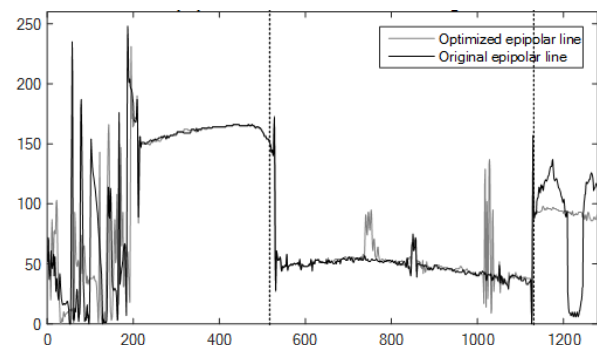|	Measure distance/mm	Absolute error/mm	Relative error/%
Matlab	243.02	1.3896	0.5718
Opencv	243.02	1.7473	0.7190
CUI [19]	243.02	0.2583	0.1063
SUN [20]	39.9876	0.0306	0.0766
proposed	236.56	0.1621	0.0685

(a) Right Image

(b) Left Image

(c) Epipolar Line 1 in Right Image

(d) Epipolar Line 1 in Left Image

Fig. 11. Epipolar matching of binocular images

6.3 Epipolar Matching of Binocular Images

In order to verify effects of above calibration, feature points are matched in a group of images collected by this calibrated binocular system after distortion correction. Then two sets of epipolar lines are obtained corresponding to these matched poles, which is shown in Fig. 11. Epipolar lines of a same pair of poles are not in the identical place before and after the fundamental matrix optimization. Subsequently, taking one pair of them for example, gray value curves on different epipolar lines in left and right images are shown in Fig. 11 (c) and (d), respectively. Light lines are optimized epipolar lines and brunet lines are original ones. From Eq. (11), it is known that positions of epipolar lines only depend on the value of the fundamental matrix F. Comparing curves among two black dotted vertical lines in both images, it can be clearly found that light curves match much better than brunet ones, which means that epipolar lines after optimization are more accurate than original ones and own higher matching degree. It follows that, in this paper, parameters of a monocular camera and external parameters of the binocular system are all close to actual ones and can meet requirements of the later high precision 3D reconstruction operation.

7 Conclusions

Based on the vanishing points orthogonality of two sets orthogonal parallel lines in space, a parameters calibration method is put forward for the binocular stereo vision system with simple operation. Due to the radial distortion that directly affects the constraint relationship between imaging points, the proposed method firstly calibrates distortion parameters of lens utilizing the centrosymmetric property of distorted images. And then, the intrinsic parameters calibration of a monocular camera is completed on the basis of the hidden feature that the length-width ratio of a reference rectangle remaining unchanged during multiple imaging. Furthermore, structure parameters are nonlinearly optimized based on the epipolar geometry constraint characteristics, which improves the accuracy of calibration results.

In experimental sections, both accuracy and stability of the distortion parameters calibration are firstly verified by processing synthetic and actually sampled images. Subsequently, effects of the binocular calibration are evaluated by the re-projection error, 3D reconstruction error of space points and matching degree of grey scale curves on a pair of epipolar lines. The experimental results show that the method in this paper overcomes low precision and poor stability of traditional ones. Only utilizing a simple and easily available calibration template, the stereo vision system can be accurately calibrated, which can even be applied to some severe conditions.

In actual measurements, it is easy to locate two sets of orthogonal parallel lines in the photographing scene. If we can obtain exact positions of some spatial points, external parameters of the system can be modified. Thus, the accuracy of the proposed method can be more precise. In the future work we will solve above problem, improve calibration speed, and realize the object 3D reconstruction.

Acknowledgements

References

[1] B. Boudine, S. Kramm, N.-E. Akkad, A. Saaidi, K. Satori, A flexible technique based on fundamental matrix for camera self-calibration with variable intrinsic parameters from two views, Journal of Visual Communication & Image Representation 39(C)(2016) 40-50.

[2] F. Yang, W. Liu, Y. Zhang, P. Gao, Z. Jia, Binocular camera calibration method combined with the four collinear constraints, Acta Optica Sinica 36(7)(2016) 0715001.

[3] O. Semeniuta, Analysis of camera calibration with respect to measurement accuracy, Procedia Cirp 41(2016) 765-770.

[4]   R. Tsai, R.-K. Lenz, A new technique for fully autonomous and efficient 3D robotics hand-eye calibration, in: the 4th international symposium on Robotics Research, 1989.

[5]   N. Sun, Y.-L. Zhang, N. Ye, H.-T. Wang, Calibration of binocular stereo measurement system based on calibration cross, Acta. Optica Sinica 32(4)(2012) 109-117.

[6]   Q. Sun, X. Wang, J. Xu, L. Wang, H. Zhang, J. Yu, Camera self-calibration with lens distortion, Optik-International Journal for Light and Electron Optics 127(10)(2016) 4506-4513.

[7]   S. Xu, X.-X. Sun, X. Liu, M. Cai, Geometry method of camera self-calibration based on a rectangle, Acta. Optica Sinica 34(11)(2014) 1115002.

[8]   Z.-Y. Zhang, A flexible new technique for camera calibration, IEEE Transactions on Pattern Analysis and Machine Intelligence 22(11)(2000) 1330-1334.

[9]   H.-C. Daniel, J. Kannala, J. Heikkilä, Joint depth and color camera calibration with distortion correction, IEEE Transactions on Pattern Analysis & Machine Intelligence 34(10)(2012) 2058-2064.

[10] J. Lu, H. Sun, Z. Chang, A novel method for camera calibration with orthogonal vanishing points, Chinese Journal of Lasers 41(2)(2014) 0208001.

[11] Y. Liu, W. Zhang, J.-H. Li, D.-O. Automation, Research status and development of key technologies of camera calibration based on vanishing points, Transducer & Microsystem Technologies 37(3)(2018) 3-13.

[12] Y. Zhao, X. Zhang, Y. Wang, L. Xu, Camera self-calibration based on circular points with two planar mirrors using silhouettes, Multimedia Tools & Applications 75(13)(2016) 7981-7997.

[13] Z. Liu, Q. Wu, S. Wu, X. Pan, Flexible and accurate camera calibration using grid spherical images, Optics Express 25(13)(2017) 15269.

[14] W. Li, S. Shan, H. Liu, High-precision method of binocular camera calibration with a distortion model, Applied Optics 56(8)(2017) 2368-2377.

[15] K.-S.-C. Kumar, A strategy for selecting optimal vergence pose and calibration patterns for stereo-vision calibration, in: Proc. IEEE International Conference on Computer Graphics, Vision and Information Security, 2016.

[16] B.-F. Zhang, C. Lu, J. Röning, W. Feng, The study of calibration and epipolar geometry for the stereo vision system built by fisheye lenses, in: Proc. SPIE 9406, Intelligent Robots and Computer Vision XXXII: Algorithms and Techniques, 2015.

[17] L.-L. Ai, F. Yuan, Z.-L. Ding, Further study on radial distortion model for photographic objective, Acta. Optica Sinica 28(10)(2008) 1930-1933.

[18] S.-Y. Wang, Research on corner detection technique for binocular vision, Mechatronics 10(2013) 36-39.

[19] Y. Cui, F.-Q. Zhou, Y.-X. Wang, L. Liu, H. Gao, Precise calibration of binocular vision system used for vision measurement, Opt. Express 22(2014) 9134-9149.

[20] H. Sun, J. Lu, Z. Chang, An efficient camera calibration and optimization method based on orthogonal vanishing points, Journal of Photographic Science 64(2016) 232-239.